Supporting Information

A thermostable calcium-based metal-organic framework for efficient capture and separation of acetylene from ternary mixture

Shan-Qing Yang,[a] Rajamani Krishna,[b] Lei Zhou,[a] Yi-Long Li,[a] Bo Xing,[a] Qiang Zhang,[a] Fei-Yang Zhang,[a] Tong-Liang Hu*[a]

[a] School of Materials Science and Engineering, National Institute for Advanced Materials, Nankai University, Tianjin 300350, China. Email: tlhu@nankai.edu.cn (T.-L. Hu)

[b] Van 't Hoff Institute for Molecular Sciences, University of Amsterdam, Science Park 904, 1098 XH Amsterdam, The Netherlands.

Experimental Section

Transient breakthrough simulations

Transient breakthrough simulations were carried out using the methodology described in earlier publications [1-5]. In these simulations, intra-crystalline diffusion influences are ignored.

The simulations were performed in a fixed bed with the following parameters: adsorber length, L = 0.3 m; cross-sectional area, A = 1 m^2; interstitial gas velocity in the bed, v = 0.1 m s^{-1}; voidage of the packed bed, ε = 0.4; the superficial gas velocity at the inlet to the bed, u = 0.04 m s^{-1}. The volumetric flow rate of the gas mixture at the inlet Q_0 = 40 L s^{-1}. The volume of MOF used in the simulations is $V_{ads} = LA(1-\varepsilon)$ = 0.18 m^3. Also, note that since the superficial gas velocity is specified, the specification of the cross-sectional area of the tube, A, is not relevant in the simulation results presented; essentially, we set A = 1 m^2. The total volume of the bed is $V_{bed} = LA$. It is important to note that the volume of adsorbent, V_{ads}, includes the pore volume of the adsorbent material. If ρ is the framework density, the mass of the adsorbent in the bed is $m_{ads} = (1-\varepsilon)\times(L \text{ m})\times(A \text{ m}^2)\times(\rho \text{ kg m}^{-3})$ kg.

For presentation of the results of the breakthrough simulations, the dimensionless concentrations at the exit, c_i/c_{i0} are plotted as a function of the dimensionless parameter $\tau = \dfrac{tu}{L\varepsilon}$, defined by dividing the actual time, t, by the characteristic time, $\dfrac{L\varepsilon}{u}$.

DFT Calculation

All density functional theory (DFT) calculations were performed using the Vienna Ab initio Simulation Package (VASP) [6,7] at the level of generalized gradient approximation (GGA) using Perdew-Burke-Ernzerhof (PBE) exchange-correlation functional [8]. Projector-augmented wave (PAW) potentials were used to describe the effective cores [9,10]. The valence electrons of all atoms were expanded in a plane wave basis set with a cutoff energy of 400 eV. The atomic structures were relaxed using either the conjugate gradient algorithm or the quasi-Newton scheme as implemented in the VASP code until the forces were less than 0.05 eV/Å for all unconstrained atoms, and the energy convergence criteria for all self-consistent field calculations were set as 10^{-4} eV. The van der Waals dispersion interaction between MOF and gas molecules was also considered by introducing the DFT-D3 method of Grimme [11]. The lattice parameters of **NUM-20** were a = 13.319 Å, b = 15.028 Å, c = 16.573 Å, so the sampling of Brillouin zone was only with Γ point [12].

The adsorption energy was defined as

$$E_{ads} = E(\text{MOF/M}) - E(\text{MOF}) - E(\text{M})$$

where the E(MOF/M), E(MOF) and E(M) represent the total energies of MOF with the adsorbate, the optimized MOF structure and the isolated gas molecules, respectively.

Fitting of Pure Component Isotherms

The isotherm data for C_2H_2, CH_4 and CO_2 in **NUM-20**, measured at 273 and 298 K were fitted with the Dual-site Langmuir-Freundlich model.

$$q = q_{A,sat}\frac{b_A p^{c_A}}{1+b_A p^{c_A}} + q_{B,sat}\frac{b_B p^{c_B}}{1+b_B p^{c_B}}$$

Calculation for C_2H_2/CH_4 and C_2H_2/CO_2 Adsorption Selectivities

The ideal adsorbed solution theory (IAST) was used to estimate the composition of the adsorbed phase from the data of single component isotherms and predict the selectivities of binary mixtures C_2H_2/CH_4 and C_2H_2/CO_2. IAST calculations of C_2H_2/CH_4 (50/50, v/v,) and C_2H_2/CO_2 (50/50, v/v) mixtures adsorption at 273 and 298 K, respectively were performed by

$$S_{ads} = \frac{q_1/q_2}{p_1/p_2}.$$

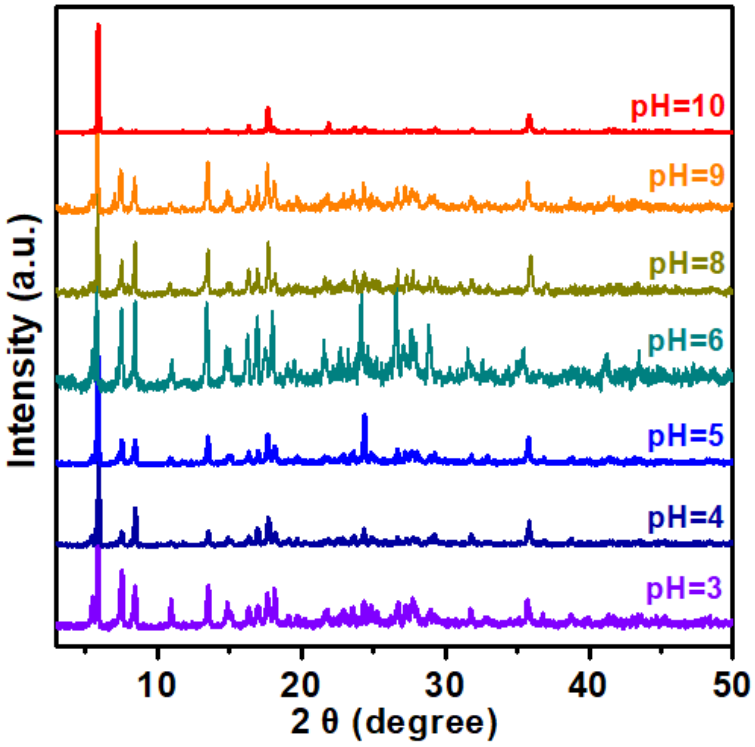

Figure S1. PXRD patterns for **NUM-20** in different pH value aqueous solutions for 12 h.

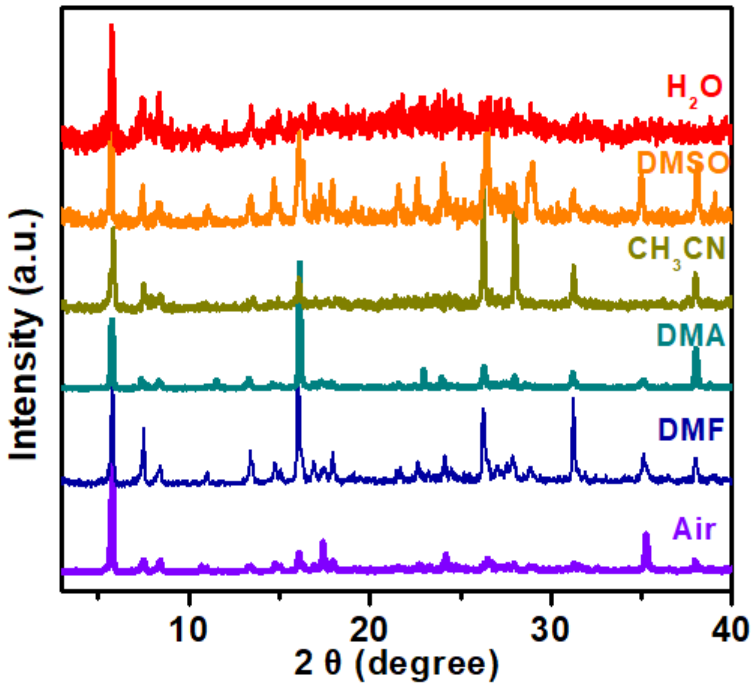

Figure S2. PXRD patterns for **NUM-20** in some organic solvents and air atmosphere for 24 h.

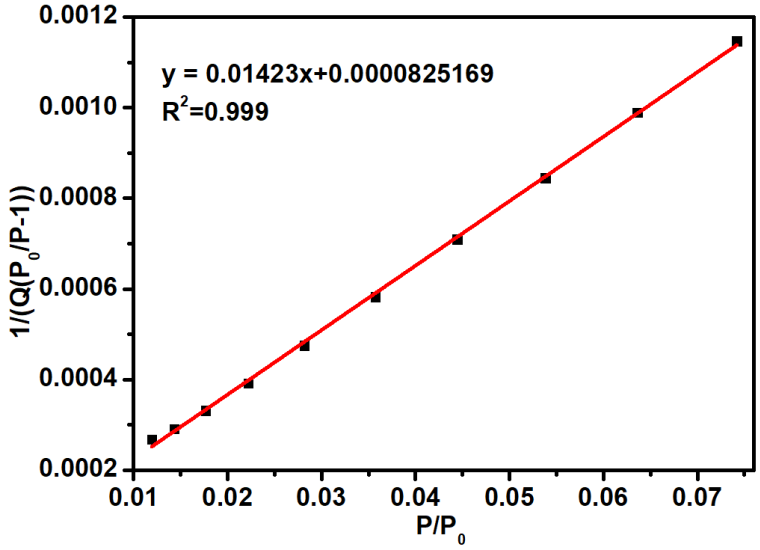

Figure S3. Calculation of BET surface area for **NUM-20** based on CO_2 adsorption isotherm at 195 K.

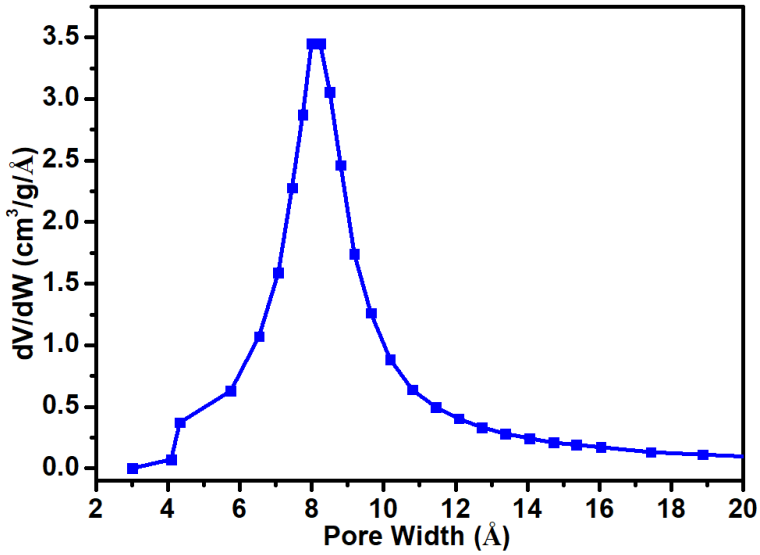

Figure S4. Pore size distribution of **NUM-20**.

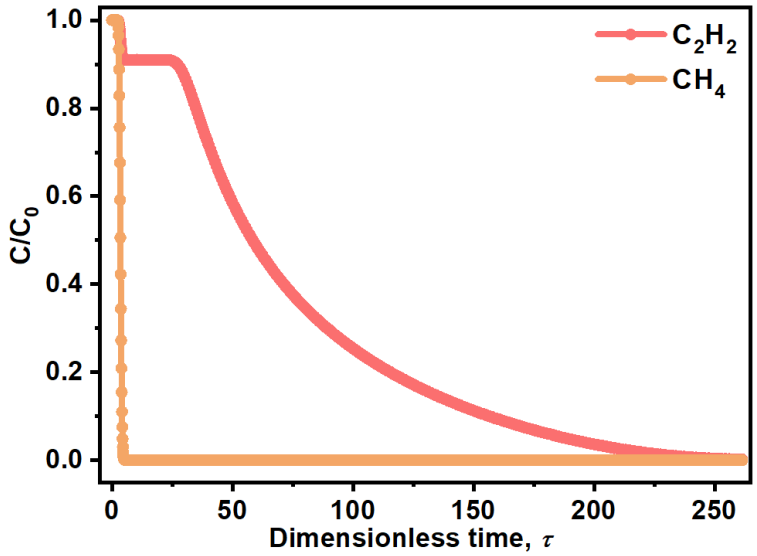

Figure S5. The desorption simulations of equimolar C_2H_2/CH_4 mixture.

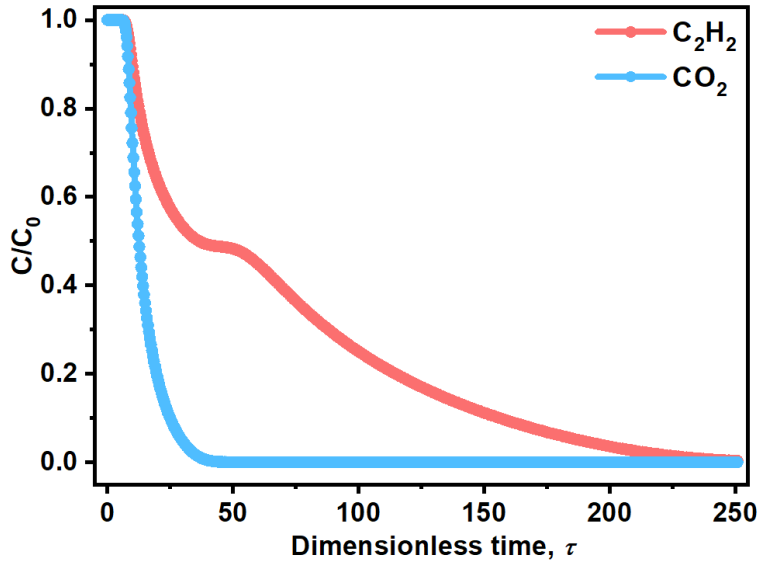

Figure S6. The desorption simulations of equimolar C_2H_2/CO_2 mixture.

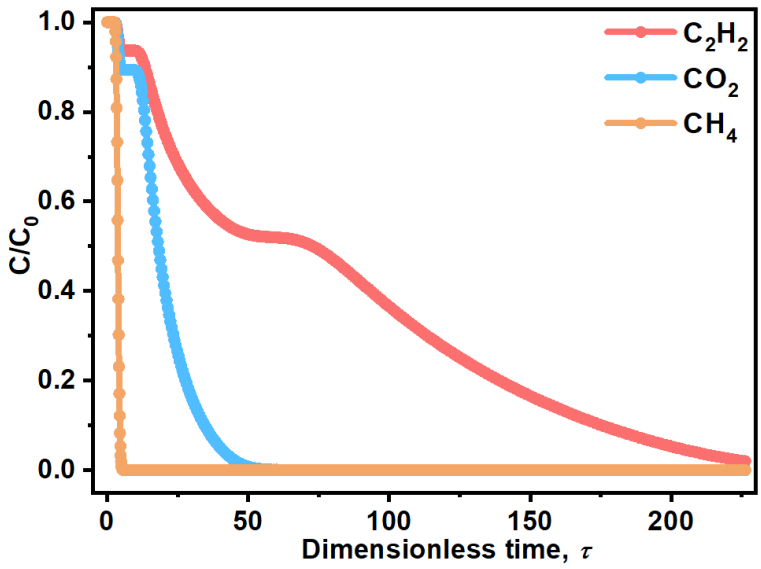

Figure S7. The desorption simulations of equimolar $C_2H_2/CH_4/CO_2$ mixture.

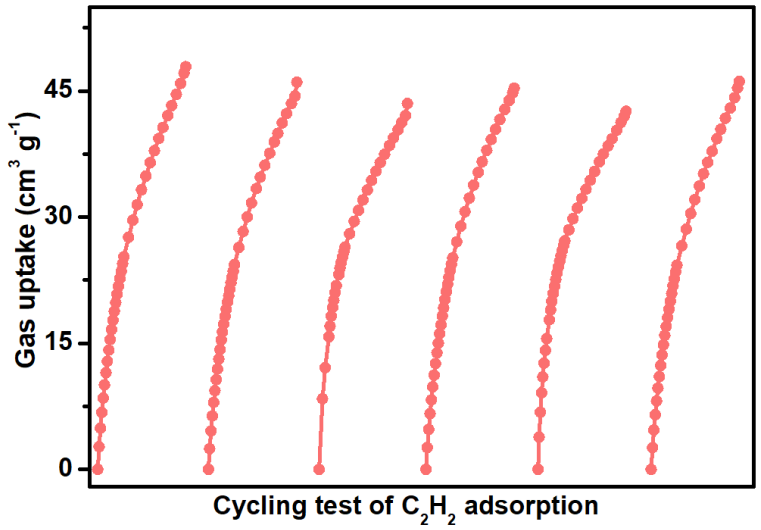

Figure S8. Cycling test of C_2H_2 adsorption measurements at 298 K.

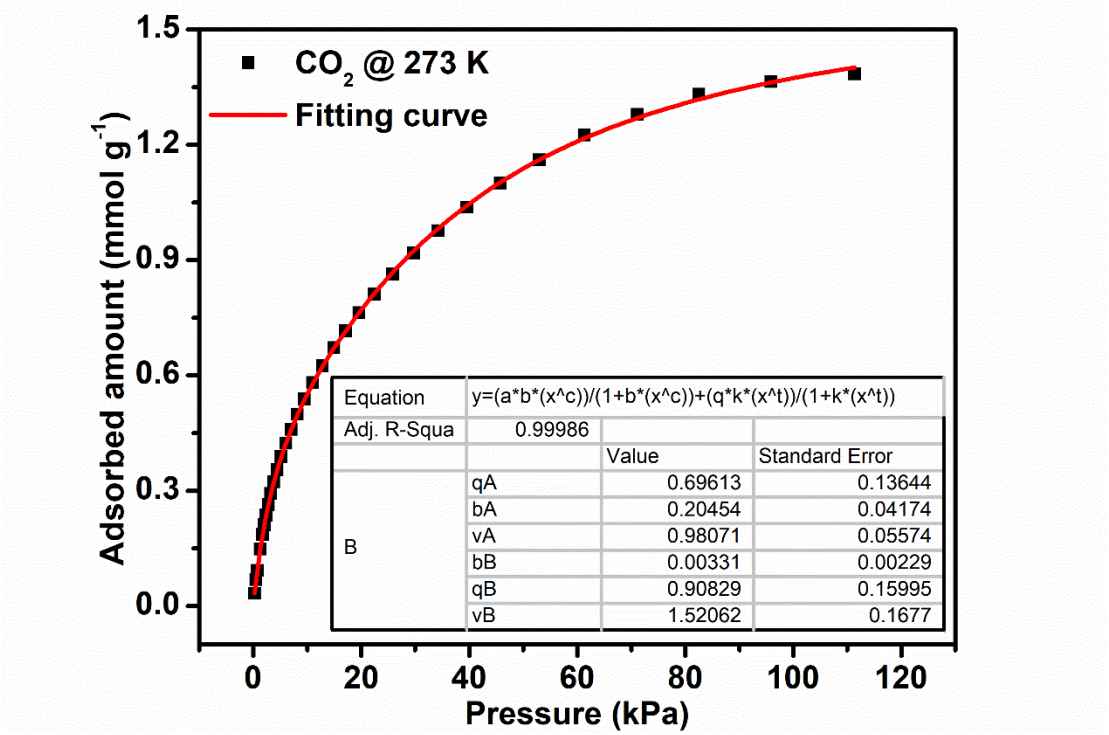

Figure S9. Dual-site Langmuir-Freundlich model for CO_2 adsorption isotherm on **NUM-20** at 273 K.

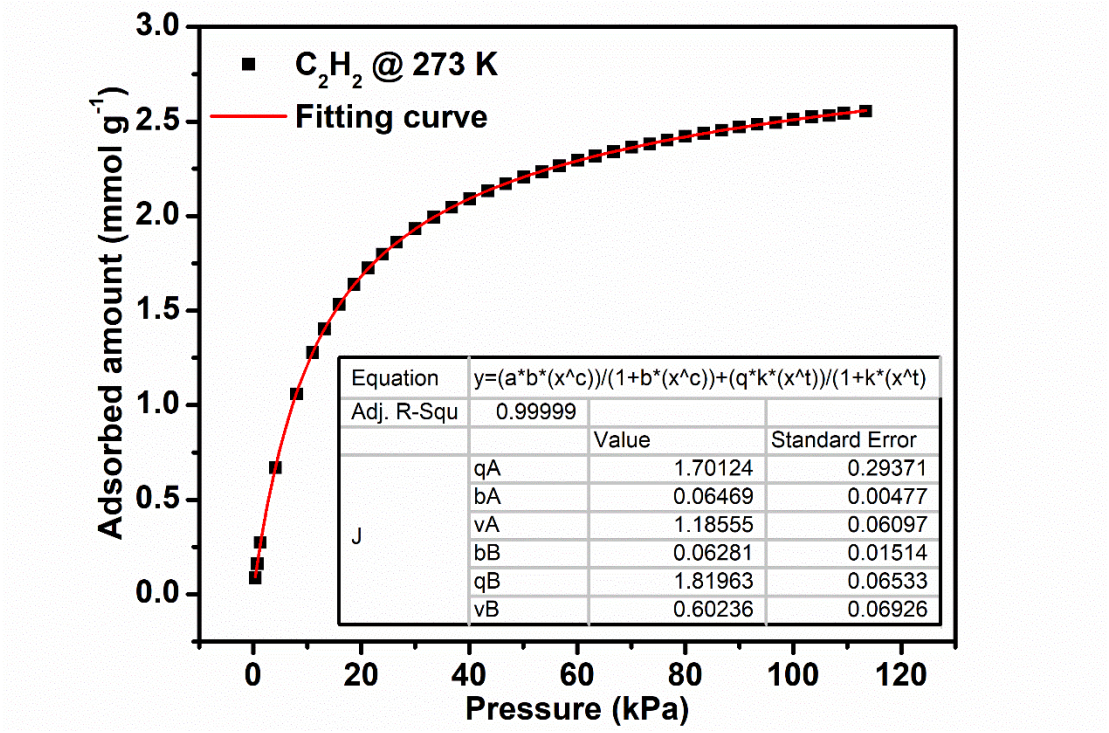

Figure S10. Dual-site Langmuir-Freundlich model for C_2H_2 adsorption isotherm on **NUM-20** at 273 K.

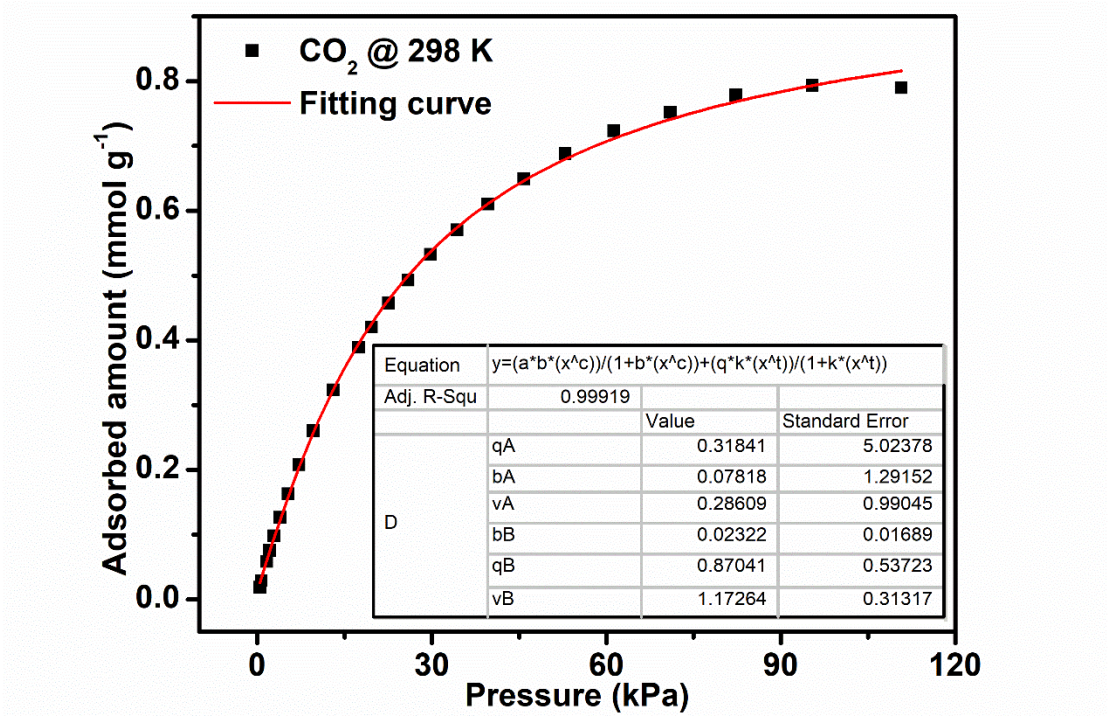

Figure S11. Dual-site Langmuir-Freundlich model for CO_2 adsorption isotherm on **NUM-20** at 298 K.

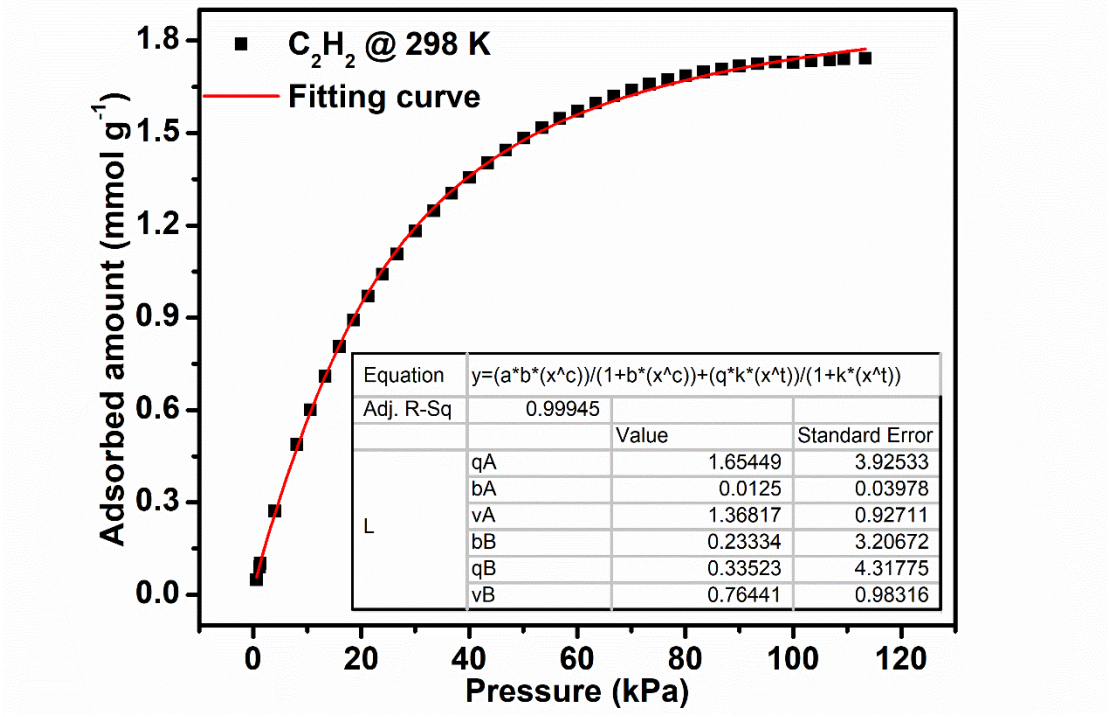

Figure S12. Dual-site Langmuir-Freundlich model for C_2H_2 adsorption isotherm on **NUM-20** at 298 K.

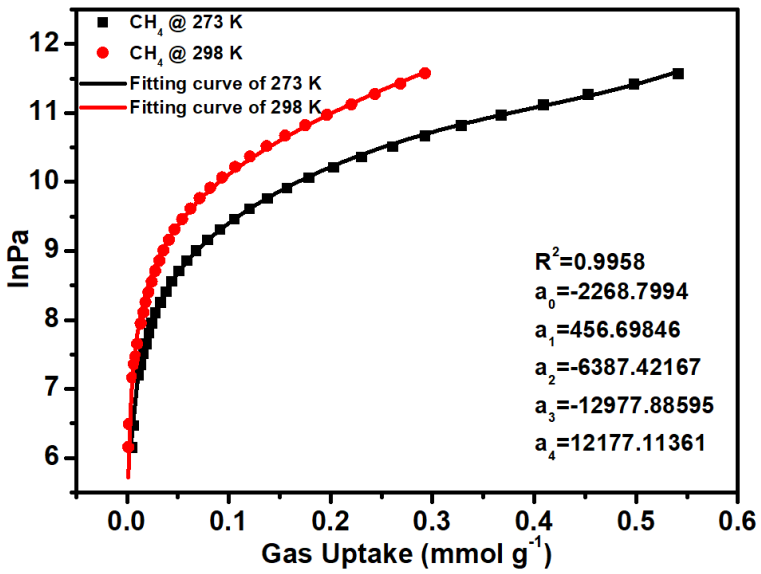

Figure S13. The details of virial equation (solid lines) fitting to the experimental CH_4 adsorption data (symbols) for **NUM-20**.

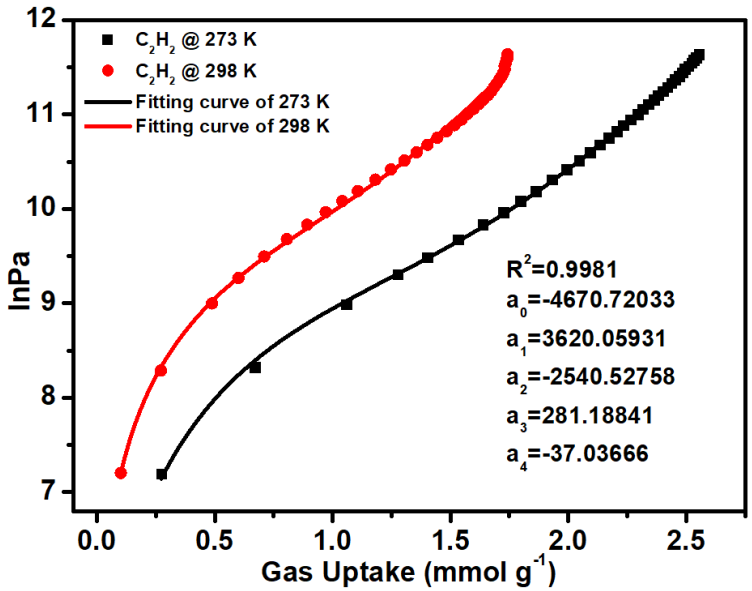

Figure S14. The details of virial equation (solid lines) fitting to the experimental C_2H_2 adsorption data (symbols) for **NUM-20**.

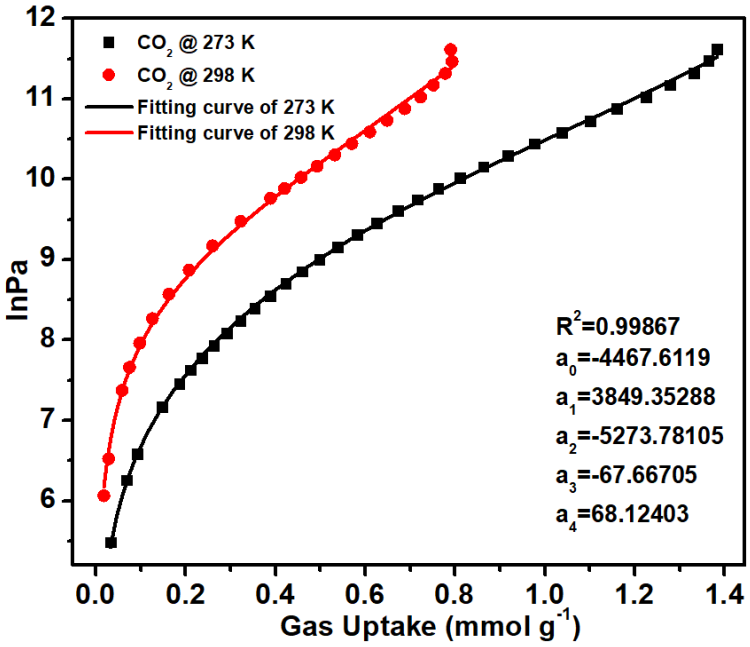

Figure S15. The details of virial equation (solid lines) fitting to the experimental CO_2 adsorption data (symbols) for **NUM-20**.

Figure S16. The DFT calculated adsorption energy of gas molecule at the site I of the **NUM-20**.

Figure S17. The DFT calculated adsorption energy of gas molecule at the site II of the **NUM-20**.

Figure S18. The DFT calculated adsorption energy of gas molecule at the site III of the **NUM-20**.

Table S1. The summary of energy of gas molecule and framework.

	C_2H_2	CO_2	CH_4	NUM-20
Energy/eV	-22.95	-23.00	-24.03	-1098.53

Table S2. The summary of energy of binding site.

	C_2H_2			CO_2			CH_4		
Site	SI	SII	SIII	SI	SII	SIII	SI	SII	SIII
Energy/ eV	-1121.65	-1121.73	-1121.76	-1121.74	-1122.03	-1121.87	-1122.70	-1122.85	-1122.81
E_{ads}/eV	-0.17	-0.25	-0.28	-0.21	-0.50	-0.34	-0.14	-0.29	-0.25

Table S3. Crystallographic parameters and refinement details of **NUM-20** ([Ca_2(TBAPy)(H_2O)$_4$·Solvents])

	NUM-20
Formula	$C_{44}H_{30}Ca_2O_{12}$
*M*r (g mol^{-1})	830.84
Crystal system	triclinic
Space group	*P*-1
a (Å)	13.3190(3)
b (Å)	15.0280(3)
c (Å)	16.5732(4)
α (°)	83.54(2)
β (°)	78.30(2)
γ (°)	89.94(2)
V (Å^3)	3226.87(1)
Z	2
D_c (g cm^{-3})	0.855
F (000)	860.0
μ (mm^{-1})	1.873
GOF on F^2	1.082
R_1, wR_2 [$I>2\sigma(I)$][a]	0.1021, 0.2908
R_1, wR_2 [all data][b]	0.1070, 0.2950

[a] $R_1 = \sum ||F_o| - |F_c|| / \sum |F_o|$. [b] $wR_2 = \{\sum[w(F_o^2 - F_c^2)^2] / \sum w(F_o^2)^2\}^{1/2}$

Table S4. A comparison of the gas adsorption and separation performance with reported adsorbents at ambient conditions.

	C_2H_2 uptake ($cm^3\ g^{-1}$)	C_2H_2/CO_2 selectivity	C_2H_2/CH_4 selectivity	Reference
$Zn(bdc)_{0.5}(mtrz)$	41.9	3.1	13.2	[13]
Cu-CPAH	131.8	3.6	20.3	[14]
$Zn_2(Pydc)(Ata)_2$	47.2	3.9	15.9	[15]
ZJU-13	115	4	20	[16]
$Zn(cpna)_3(tmbpy)$	71.25	3.9	22.4	[17]
NbU-11	77.3	2.5	175.8	[18]
Ni(dpip)	83.6	2	16.6	[19]
BUT-318a	51.46	5.5	105.8	[20]
BSF-1	52.5	3.3	46.9	[21]
SNNU-63	91.1	3.3	12.9	[22]
FJU-36a	52.2	2.8	17.7	[23]
NUM-20	39.03	5.4	99.3	This work

References

[1] R. Krishna, The Maxwell-Stefan description of mixture diffusion in nanoporous crystalline materials, Micropor. Mesopor. Mater. 185 (2014) 30-50.

[2] R. Krishna, Methodologies for evaluation of metal-organic frameworks in separation applications, RSC Adv. 5 (2015) 52269-52295.

[3] R. Krishna, Screening metal-organic frameworks for mixture separations in fixed-bed adsorbers using a combined selectivity/capacity metric, RSC Adv. 7 (2017) 35724-35737.

[4] R. Krishna, Methodologies for screening and selection of crystalline microporous materials in mixture separations, Sep. Purif. Technol. 194 (2018) 281-300.

[5] R. Krishna, Metrics for evaluation and screening of metal-organic frameworks for applications in mixture separations, ACS Omega 5 (2020) 16987-17004.

[6] G. Kresse, J. Furthmüller, Efficient iterative schemes for ab initio total-energy calculations using a plane-wave basis set, Phys. Rev. B: Condens. Matter Mater. Phys. 54 (1996) 11169.

[7] G. Kresse, J. Furthmüller, Efficiency of ab-initio total energy calculations for metals and semiconductors using a plane-wave basis set, Comput. Mater. Sci. 6 (1996) 15-50.

[8] J.P. Perdew, K. Burke, M. Ernzerhof, Generalized gradient approximation made simple, Phys. Rev. Lett. 77 (1996) 3865.

[9] G. Kresse, D. Joubert, From ultrasoft pseudopotentials to the projector augmented-wave method, Phys. Rev. B: Condens. Matter Mater. Phys. 59 (1999) 1758.

[10] P. E. Blöchl, Projector augmented-wave method, Phys. Rev. B: Condens. Matter Mater. Phys. 50 (1994) 17953.

[11] S. Grimme, J. Antony, S. Ehrlich, H. Krieg, A consistent and accurate ab initio parametrization of density functional dispersion correction (DFT-D) for the 94 elements H-Pu, J. Chem. Phys. 132 (2010) 154104.

[12] H. J. Monkhorst, J.D. Pack, Special points for Brillouin-zone integrations, Phys. Rev. B: Condens. Matter Mater. Phys. 13 (1976) 5188.

[13] Z.-H. Wang, R.-H. Su, G.-D. Wang, W.-J. Shi, L. Hou, Methyl-functionalized Zn-MOF for selective adsorption and separation of acetylene, J. Environ. Chem. Eng. 11 (2023) 110488.

[14] L. Meng, L. Yang, C. Chen, X. Dong, S. Ren, G. Li, Y. Han, Z, Shi, S. Feng, Selective acetylene adsorption within an imino-functionalized nanocage-based metal-organic framework, ACS Appl. Mater. Interfaces 12 (2020) 5999-6006.

[15] N. Xu, Y. Jiang, W. Sun, J. Li, L. Wang, Y. Jin, Y. Zhang, D. Wang, S. Duttwyler, Gram-scale synthesis of an ultrastable microporous metal-organic framework for efficient adsorptive separation of C_2H_2/CO_2 and C_2H_2/CH_4, Molecules 26 (2021) 5121.

[16] X. Duan, T. Xia, Z. Ji, Y. Cui, Y. Yang, G. Qian, A new microporous metal-organic framework for highly selective C_2H_2/CH_4 and C_2H_2/CO_2 separation at room temperature, Chin. J. Chem. 35 (2017) 1289-1293.

[17] P. Yan, J. Yang, X. Hao, Z. Chen, G. Shen, Y. Zhao, D. Ma, J. Zhu, A microporous zinc–organic framework with Lewis basic pyridyl sites for highly selective C_2H_2/CH_4 and C_2H_2/CO_2 gas separation, CrystEngComm 22 (2020)275-282.

[18] N. Wu, Q. Li, J. Li, D. Wu, Y. Li, 4-Connected cobalt-based 3D framework with a high affinity for acetylene, Inorg. Chem. 59 (2020) 9461-9464.

[19] Y.-Z. Li, G.-D. Wang, L.-N. Ma, L. Hou, Y.-Y. Wang, Z. Zhu, Multiple functions of gas separation and vapor adsorption in a new MOF with open tubular channels, ACS Appl. Mater. Interfaces 13 (2021) 4102-4109.

[20] Z.-C. Xu, J. Yu, P.-D. Zhang, Y.-L. Zhao, X.-Q. Wu, M. Zhao, X. Zhang, J.-R. Li, Efficient C_2H_2 separation from CO_2 and CH_4 within a microporous metal-organic framework of multiple functionalities, Ind. Eng. Chem. Res. 61 (2022) 16233-16239.

[21] Y. Zhang, L. Yang, L. Wang, S. Duttwyler H. Xing, A microporous metal-organic framework supramolecularly assembled from a Cu(II) dodecaborate cluster complex for selective gas separation. Angew. Chem. Int. Ed. 58 (2019) 8145-8150.

[22] Y.-T. Li, J.-W. Zhang, H.-J. Lv, M.-C. Hu, S.-N. Li, Y.-C. Jiang, Q.-G. Zhai, Tailoring the pore environment of a robust Ga-MOF by deformed $[Ga_3O(COO)_6]$ cluster for boosting C_2H_2 uptake and

separation, Inorg. Chem. 59 (2020) 10368-10373.

[23] L. Liu, Z. Yao, Y. Ye, L. Chen, Q. Lin, Y. Yang, Z. Zhang, S. Xiang, Robustness, selective gas separation, and nitrobenzene sensing on two isomers of cadmium metal-organic frameworks containing Various metal-O-metal chains, Inorg. Chem. 57 (2018) 12961-12968.